



Morphology differences between fractional Brownian motion and the Weierstrass-Mandelbrot function and corresponding Hurst evaluation

Jiabin Dong · Ying Wu · Yi Jin · Shunxi Liu · Junling Zheng · Wenhao Dong

Received: 15 September 2022 / Accepted: 3 December 2022
© The Author(s) 2023

Abstract Fractional Brownian motion (FBM) and the Weierstrass-Mandelbrot (W-M) function are two important methods for constructing self-affine objects. Accurately characterizing their features, such as the morphology and fractal geometry, is fundamental for their follow-up applications. However, due to the differences between self-similar and self-affine properties, the fractal dimension evaluation is difficult and sometimes unconvincing. In addition, the sampling length and diversity of calculation methods both lead to the non-uniqueness of the fractal dimension. This study compared the morphology

differences between FBM and the W-M function and then analyzed the effects of each parameter on their morphology. Comparisons indicated that FBM has fewer control parameters than the W-M function. Finally, from basic fractal geometric properties, we derived the relationship between the measurement scale r and profile lengths $L(r)$ for self-affine profiles and found that it is a complicated form rather than $L(r) \sim cr^{H-1}$, where H is the Hurst exponent. Meanwhile, the equivalent vertical height $v(r)$ has an intuitive and clear power law relationship to the measurement scale $v(r) \sim \sigma r^H$, which provides a method to estimate the Hurst exponent.

J. Dong · Y. Wu · Y. Jin · S. Liu · J. Zheng · W. Dong
School of Resources and Environment, Henan Polytechnic University, 2001 Century Avenue, Jiaozuo 454003, Henan, China
e-mail: jiajunfengbin@hpu.edu.cn

Y. Wu
e-mail: wuying@hpu.edu.cn

S. Liu
e-mail: lsx@hpu.edu.cn

J. Zheng
e-mail: zhengjun.ling@163.com

W. Dong
e-mail: dongwh1998@163.com

Y. Jin (✉)
Collaborative Innovation Center of Coal Work Safety and Clean High Efficiency Utilization, Henan Polytechnic University, 2001 Century Avenue, Jiaozuo 454003, Henan, China
e-mail: jinyi2005@hpu.edu.cn

Highlights

- Clarified improper use of parameters in W-M function that causes the deviation of D
- The total length $L(r_h)$ and measured scale r_h satisfy $L(r_h) = \lambda_0^*(1 + \sigma^2(r_h)^{2H-2})^{1/2}$
- Decomposed the scaling lacunarity of rough profiles and derived the estimation of D

Keywords Fractional Brownian motion · Weierstrass-Mandelbrot function · Hurst evaluation · Fractal geometry properties

1 Introduction

The irregular roughness of rock fractures critically affects rock strength and fluid flow through rock media (Zhao et al 2018; Jin et al 2017a; Zhao et al 2021; Zimmerman et al 1991). Numerous researchers have studied quantitative descriptions. Previous research has verified that rock fracture surfaces satisfy self-affine scaling characteristics (Odling 1994; Mandelbrot 1967; Gao et al 2021; Liu et al 2021; Yang et al 2021). The characterization of surface roughness is thus a basic prerequisite for further analysis.

In addition to real rock fractures (Zhang et al 2020, 2019; Dong and Ju 2020), the Weierstrass-Mandelbrot (W-M) function and fractional Brownian motion (FBM) are two important methods for generating self-affine rough profiles or surfaces with random features (Ausloos M et al 1985; Berry et al 1980; Eliazar and Shlesinger 2013; Mandelbrot and Van Ness 1968; Chen et al 2018). In addition, they have been widely applied to simulate rough surfaces such as rock fracture surfaces, road surfaces, and milling surfaces (Ju et al 2019; Pinnington 2012; Zheng et al 2020; Zhou et al 2015; Zuo et al 2015; Yan and Komvopoulos 1998; Yin and Komvopoulos 2010). For example, Jin et al (2017a) applied a W-M function to study fluid flow through self-affine fractures. Using the successive random additions method, Dou et al (2019) studied solute transport through rough flow channels. In fact, the randomized W-M function is a similar process to FBM. Their self-affine properties can be described using the Hurst exponent H (Falconer 2014; Dou et al 2018a). In addition, the sampling length of a profile has important effects on the fractal dimension (Zuo et al 2020; Zhang et al 2021). Thus, it is important to check their morphology and whether the constructed profiles satisfy the designed self-affine properties i.e., whether the calculated H of these profiles is equal to the set H .

The Hurst exponent plays an important role in characterizing the scale invariance of a fractal profile (Zhao et al 2020; Zuo et al 2015). Accurately evaluating H is the basis for characterizing the fractal properties of complex objects and their subsequent applications (Cai et al 2013, 2018; Xu 2015; Costa 2006; Dou et al 2018b). Therefore, starting from the geometrical meaning of each parameter of the fractal processes, we extensively analyzed and assessed the H calculation method of 2D self-affine profiles.

To date, scholars have proposed numerous methods for calculating H of rough profiles. Among them, the most classic method is the divider method proposed by Mandelbrot (1967), which analyzes the number-scale relationship. This method is widely accepted for its simplicity and intuitive physical meaning (Zhang et al 2020; Yu 2006; Yu and Li 2001). However, the number-scale relationship has its shortcomings and limitations (Odling 1994; Ganti and Bhushan 1995; Jin et al 2017b). The measured number and length are affected by the starting point of the measurement. Sugihara et al (1990) suggested choosing different starting points to obtain the average length to weaken the influence of the starting point. Later, Babadagli and Develi (2003) even pointed out that there is no effective method for evaluating the fractal properties of all fractal surfaces.

In addition to the divider method, box-counting methods (Li et al 2009; Karle and Kolwankar 2015; Feranie et al 2011; Ficker 2017), power spectral density (Babadagli and Develi 2003; Ünlüsoy and Süzen 2020), three-point sinuosity (Zhou et al 2015), and other methods (Zhao et al 2018; Ban et al 2021; Liu et al 2017; Wu 2002) have been proposed to revise the evaluation of H . The most famous method is box-counting, which is frequently applied to calculate the fractal dimension of pore structures and fractal profiles (Xia et al 2018; Xu et al 2016). Most of the above methods are effective only for self-similar objects, and their effectiveness for self-affine fractals is limited (Jin et al 2019; Zuo et al 2015; Ficker 2017). To expand the fractal dimension evaluation method, Dong et al (2017) derived an evaluation method for self-affine profiles by expanding Brown's magnifying method (Brown 1987). Their results indicated that the calculated H of the W-M profiles deviates from the set H in the function, which leads to the idea of comparing the W-M function and FBM in this study. In terms of fractal theory, Jin et al (2017b, 2019) derived a Hurst model based on the fractal topography for characterizing the scale-invariance in different directions. Their research unified the definition of self-similar, self-affine, single- and multiphase properties, which provides methods for calculating the Hurst exponent of self-affine fractals. However, this has not been tested on actual rough profiles or self-affine functions such as FBM and the W-M function.

The W-M function has been widely applied for generating rough profiles in many fields (Zhang et al

2021; Jin et al 2017a; Ju et al 2019; Chen et al 2018); however, it has some drawbacks. Wu (2000) indicated that W-M surfaces and natural surfaces were different by comparing their spectral densities. Dong et al (2017) studied the evaluation of fractal dimensions of W-M profiles and found that the evaluated fractal dimensions deviated from the set values, especially for objects with a small fractal dimension. In addition, the number of variables in the function is relatively large, which increases the difficulties in its application. Chen et al (2018) compared the four methods for estimating fractal dimensions of the Weierstrass-Mandelbrot function, and they found that none of the methods is particularly prominent in all three aspects. Zuo et al (2020) pointed out that the sampling length also plays a crucial role in affecting fractal dimension calculations. Therefore, it is of crucial importance to assess the controlling mechanism of each variable on profile morphology and evaluate the fractal dimensions of rough profiles.

This research first compared the morphological differences between W-M profiles and FBM profiles. The results indicate that the W-M function, different from FBM, is dominated by more parameters. Specifically, once H , the random characterization, and the step are determined, one can obtain the unique FBM profile. However, this is not the case for the W-M function. Then, based on the basic geometric relationship and fractal properties, this study derived a length model and determined its relationship with the Hurst exponent and measuring scale. By comparing it with the classic length-size relationship (Mandelbrot 1967), we distinguished the difference between self-similar and self-affine fractals. For self-affine objects, the measured length and the measuring scale obey a more complicated relationship rather than the classic length-size relationship. Meanwhile, the equivalent vertical length, calculated based on the length model, was proven to obey the power law relationship with the horizontal length, the exponent of which is the Hurst exponent.

Further explorations of the equivalent vertical length and the horizontal length verified that the power exponent between the two scaling lacunarities determined the Hurst exponent. With the above relationships, the Hurst exponent of the FBM profiles was evaluated. A comparison with the set H of FBM profiles verified the fractal characteristics of FBM. However, the study shows that the Hurst results of

W-M function have diversity; that is, for some appropriate parameters, the results match well, but for other parameters, the data match is not as good. These comparisons and analyses indicate that the fractal properties of the W-M function are dominated not only by H but also by the low- and high-frequency range of waves. This paper mainly derives the H evaluation method for self-affine profiles. This model solves the problem of the deviation between the evaluated H and the set value. Which provides a method reference for the fractal characterization and description of rough profiles.

2 Methods

2.1 Fractional Brownian motion

Fractional Brownian motion (FBM) is a generalization of classic Brownian motion (Magdziarz et al 2009), and Brownian motion is a stochastic process with increments satisfying a stationary, independent Gaussian distribution. Brownian motion was first constructed mathematically by Wiener (1923). Here, we used $X(t)$ to note such a time series of Brownian motion. $X(t)$ represents the position at time t and starts at $t = 0$ ($X(0) = 0$). For any time $t > 0$ and time interval τ , the increment ($X(t + \tau) - X(t)$) from t to $t + \tau$ is nearly a Gaussian distribution with a probability density function $P(u)$ as:

$$P(u) = \frac{1}{\sigma\sqrt{2\pi\tau}} e^{\left(\frac{-u^2}{2\tau\sigma^2}\right)}, \tag{1}$$

where σ represents the volatility of the process. $X(t)$ is a continuous function of t ; for all $t \geq 0$ and $\tau > 0$, its increment ($X(t + \tau) - X(t)$) thus satisfies:

$$P(X(t + \tau) - X(t) \leq x) = \frac{1}{\sigma\sqrt{2\pi\tau}} \int_{-\infty}^x e^{\left(\frac{-u^2}{2\tau\sigma^2}\right)} du, \tag{2}$$

if $\gamma > 0$, by replacing τ with $\gamma\tau$ and x with $\gamma^{1/2}x$, we can obtain:

$$P(X(\gamma(t + \tau)) - X(\gamma t) \leq \gamma^{1/2}x) = P(X(t + \tau) - X(t) \leq x). \tag{3}$$

Thus, $X(t)$ and $\gamma^{-1/2}X(\gamma t)$ have the same distribution. This means that one can obtain the same statistical distribution as the original if scaling the time by γ

and the spatial scale by $\gamma^{1/2}$. This is the statistically self-affine property of Brownian motion if we treat time t as a parameter. From another point of view, if one treats $X(t)$ as a set $\{X(t) : 0 \leq t \leq T\}$ rather than $\{(t, X(t)) : 0 \leq t \leq T\}$. Then, the Brownian motion is statistically self-similar since the spatial distribution of the set $\{X(t) : 0 \leq t \leq T\}$ is indistinguishable to the set $\{X(t) : 0 \leq t \leq \gamma T\}$ by scaling $\gamma^{1/2}$.

Different from that of the Brownian motion, the increment $(X(t + \tau) - X(t))$ of FBM is a normal distribution with mean 0 and variance τ^{2H} ; thus:

$$P(X(t + \tau) - X(t) \leq x) = \frac{1}{\sigma \tau^H \sqrt{2\pi}} \int_{-\infty}^x e^{\left(\frac{-u^2}{2\sigma^2 \tau^{2H}}\right)} du. \tag{4}$$

The difference between Eqs. (2) and (4) is the exponent of τ . When $H = 1/2$, Eq. (4) degenerates into Eq. (2). $\gamma^{-H}X(\gamma t)$ has the same statistical distribution as $X(t)$ when $\gamma > 0$. With $E(X(t)^2) = \sigma^2 t^{2H}$ and $E((X(t + \tau) - X(t))^2) = \sigma^2 \tau^{2H}$ (Dou et al 2018a, b), we can obtain $E(X(t + \tau)X(t)) = \sigma^2 [(t + \tau)^{2H} + t^{2H} - \tau^{2H}]/2$, and then

$$E(X(t)(X(t + \tau) - X(t))) = \frac{\sigma^2}{2} [(t + \tau)^{2H} - t^{2H} - \tau^{2H}]. \tag{5}$$

$E((X(t) - X(0))(X(t + \tau) - X(t))) > 0$ if $H > 1/2$. This indicates that $X(t + \tau) - X(t)$ and $X(t) - X(0)$ trend to be of the same sign. When $H < 1/2$, they tend to have opposite signs. If $H = 1/2$, $X(t + \tau) - X(t)$ and $X(t) - X(0)$ are independent. This independent property complicates the simulation of fractional Brownian motion. Randomizing the Weierstrass function is an alternative method to construct random processes with characteristics similar to exponent- H fractional Brownian motion.

2.2 Weierstrass-Mandelbrot function

Mandelbrot (1977) and Berry et al (1980) indicated that the Weierstrass function is a fractal. The Weierstrass function has no smallest scale but has a largest scale, which hinders its application in simulating fractal phenomena. To generalize this function, Mandelbrot extended it into a form with no scale:

$$W(t) = \sum_{n=-\infty}^{\infty} \frac{(1 - e^{it\gamma^n})e^{i\phi_n}}{\gamma^{(2-D)n}} \tag{6}$$

$(1 < D < 2, \gamma > 1, \phi_n = \text{arbitrary phases})$

$W(t)$ is a function of t , and Eq. (6) is complex. D is the fractal dimension of real part $\text{Re } W(t)$ and imaginary part $\text{Im } W(t)$. ϕ_n is the random item that controls the deterministic and stochastic behavior of $W(t)$. γ is the rescaling factor that controls the density distribution of frequencies and is often set as 1.5. With the restricted parameters, the series of $W(t)$ converges, but its derivation does not. Due to the important contribution of Mandelbrot, this function was therefore latter called the Weierstrass-Mandelbrot (W-M) function. For the convenience of applications, $\text{Re } W(t)$ is rewritten as (Ausloos M et al 1985; Berry et al 1980; Yin and Komvopoulos 2010):

$$W(t) = A \sum_{n=-\infty}^{\infty} \frac{\cos(\phi_n) - \cos(2\pi\gamma^n t/L_s - \phi_n)}{\gamma^{(2-D)n}}, \tag{7}$$

where L_s represents the characteristic length. In actual applications, it is unrealistic to set the upper and lower limits of the overlay to infinity. Therefore, the lower and upper limits are set as N_l and N_h according to the corresponding problem. In addition, A before the summation plays a role in adjusting the amplitude of the profiles. $2 - D$ in this equation plays a similar role as H in Eq. (4). However, the choice of N_l and N_h and the distribution of random items will cause differences in the fractal graph and the derivation of the fractal dimension. This phenomenon will be explained in Sect. 3.

2.3 Estimation of H for self-affine profiles

As explained in Sect. 2.1, the graphs of FBM and the W-M function are self-affine since the t -axis is treated as the parameter with a real physical meaning. For self-affine profiles, the calculation of fractal dimension is difficult due to the different scaling properties in different directions. The divider method and its derivations have been widely applied to evaluate the fractal dimension for rough profiles. This method calculates D by analyzing the relationship between the divider step (r) and the total length ($L(r)$) as follows:

$$L(r) \sim cr^{1-D}. \tag{8}$$

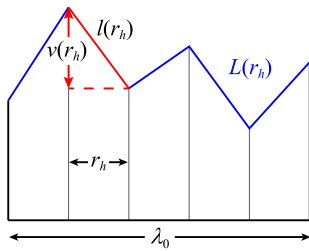


Fig. 1 Terms used to evaluate the length of a self-affine profile

With the power law relationship in Eq. (8), one can obtain the fractal dimension D of a rough profile. This is, however, only an approximation for self-similar objects, which is not suitable or should be carefully implemented, at least for self-affine fractals (Jin et al 2017b, 2019; Wong 1987). When evaluating the fractal properties of self-affine profiles, the most important task is to determine the scaling lacunarity P in different directions (Jin et al 2017b, 2019). In other words, it is to extract the attribute information in different axes. For example, Brown (1987) expanded the vertical height of self-affine profiles to conceal the horizontal length effects. For a self-affine profile, its length can be evaluated from a simple geometric relationship:

$$l(r_h)^2 = r_h^2 + v(r_h)^2, \quad L(r_h) = \frac{\lambda_0}{r_h} * l(r_h), \tag{9}$$

where $l(r_h)$ represents the length of one segment with a horizontal length of r_h and a corresponding vertical height of $v(r_h)$. Therefore, the profile length $L(r_h)$ is equal to the product of $l(r_h)$ and the segment number λ_0/r_h , where λ_0 is the horizontal length. The meaning of each parameter can be found in the following figure (Fig. 1):

As explained in 2.1, the difference expectation between two adjacent positions of FBM satisfies $E((X(t + \tau) - X(t))^2) = \sigma^2 \tau^{2H}$. $E((X(t + r_h) - X(t))^2) = \sigma^2 r_h^{2H}$ when $\tau = r_h$, and therefore, $L(r_h)$ in Eq. (9) can be written as:

$$L(r_h) = \lambda_0 * \sqrt{1 + \sigma^2 r_h^{2H-2}}. \tag{10}$$

From the above equation, it is known that $L(r_h)$ and r_h satisfy:

$$\left(\frac{L(r_h)}{\lambda_0}\right)^2 - 1 = \sigma^2 r_h^{2H-2}, \tag{11}$$

where λ_0 and σ have fixed values for a self-affine profile; therefore, $L(r_h)$ seems to have a power relationship with r_h . However, when compared with $L(r) \sim cr^{1-D} = cr^{H-1}$, we find that the main difference concentrates on the left-hand side of Eq. (11). In fact, Eq. (11) can be written as:

$$\frac{L(r_h)^2 - \lambda_0^2}{\lambda_0^2} = \sigma^2 r_h^{2H-2}, \tag{12}$$

where the left-hand side is the ratio of $(L(r_h)^2 - \lambda_0^2)$ to λ_0^2 , which can be regarded as the square of the ratio of vertical height to horizontal length. While the form of Eq. (8) is $L(r)^2 \sim cr^{2H-2}$, the comparison between them verifies the difference between self-similar fractals and self-affine fractals. From the comparison, it is known that one has to separate attribute information in different directions when evaluating fractal properties of self-affine objects.

λ_0 in Eq. (12) can be replaced by $N(r_h) * r_h$ with $N(r_h) = \lambda_0/r_h$. By dividing the numerator and denominator on the left-hand side of Eq. (12) by $N(r_h)^2$, one can obtain Eq. (13):

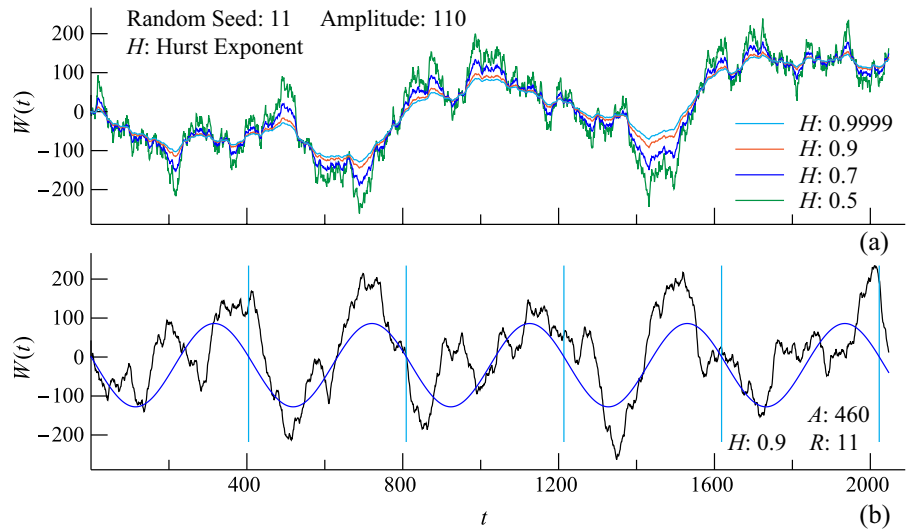
$$\frac{l(r_h)^2 - r_h^2}{r_h^2} = \frac{v(r_h)^2}{r_h^2} = \sigma^2 r_h^{2H-2}. \tag{13}$$

Equation (13) transforms to $v(r_h) = \sigma r_h^H$. In fact, this equation is similar to the variogram method in Chen et al (2018); however, we derived its essential form here. With this equation, the Hurst exponent can be evaluated by:

$$H = \frac{1}{\log \sigma} \frac{\log v(r_h)}{\log r_h} \sim \frac{\log v(r_h)}{\log r_h}. \tag{14}$$

The maximum horizontal length is λ_0 (marked as $r_{h,0}$ here), and we mark the maximum vertical length as $v_{\max} = v(r_{h,0})$. The horizontal length and vertical length of the next level are $r_{h,1}$ and $v(r_{h,1})$, respectively. These two values of the i^{th} level are marked as $r_{h,i}$ and $v(r_{h,i})$. Therefore, the scaling lacunaritys (P_h, P_v) in the horizontal and vertical directions are $P_v = v(r_{h,i})/v(r_{h,i+1})$ and $P_h = r_{h,i}/r_{h,i+1}$, respectively. With $v(r_h) = \sigma r_h^H$, the following relationship is obtained:

Fig. 2 **a** The comparison of W-M profiles of different Hurst exponents when $N_l = 0$; **b** The morphology of a rough profile with $N_l = 4$, $H = 0.9$, $A = 460$, and random seed of 11, and the blue curve represents the cosine with period of $2\pi/(2\pi\gamma^{N_l}/L_s) = L_s/\gamma^4 \approx 404.54$



$$P_v = \frac{v(r_{h,i})}{v(r_{h,i+1})} = \frac{\sigma r_{h,i}^H}{\sigma r_{h,i+1}^H} = \left(\frac{r_{h,i}}{r_{h,i+1}} \right)^H = P_h^H, \quad (15)$$

and therefore $H = \log P_v / \log P_h$, which is the same as that derived by Jin et al in Refs. (Jin et al 2017b, 2019, 2020). Equations (11) and (14) provide methods to evaluate the Hurst exponent of self-affine profiles, and the comparison will be discussed in the results and discussion section.

3 Results and discussion

3.1 Morphology differences in the FBM and W-M graphs

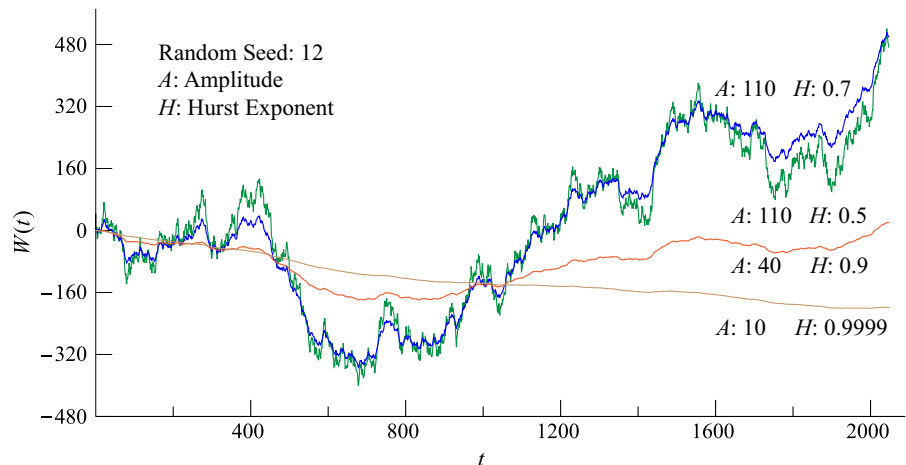
The morphology of a W-M fractal rough profile is determined by the comprehensive effects of many parameters, such as N_l , A , L_s , $2 - D$, ϕ_n , N_h , and the simulated length of a profile. Next, we discuss the effects of each parameter on the profile morphology. From Eq. (7), it is known that the rough profile is composed of the sum of different-period cosines. The period of cosines is determined by N_l , γ , and L_s , with the minimal positive period of cosines equal to $2\pi/(2\pi\gamma^{N_l}/L_s)$. For all the cosines in Eq. (7), the largest value of the minimal positive periods is $2\pi/(2\pi\gamma^{N_l}/L_s)$. In this research, we set $L_s = 2048$ as a dimensionless parameter. The simulated length is set as a list ranging from 0 to 2047 with a step equal

to 1, which means that one fractal profile is dominated by 2048 points (the same as L_s) in total.

To illustrate the effects of N_l on the periodicity of a profile, we compared W-M graphs of different N_l (0 and 4) but the same $N_h = 50$ (Note: $N_h = 50$ is used in the following study because its effects on profiles are relatively small when N_h is much larger than N_l) in Fig. 2. The N_l values in Fig. 2a and b are 0 and 4, respectively. When $N_l = 0$, it is easy to obtain $2\pi/(2\pi\gamma^{N_l}/L_s) = L_s$, which means the minimal period the function is equal to L_s . Here, both L_s and the sampling length are equal to 2048, which means that the profiles are of one period.

Then, by increasing $N_l = 4$, we obtained another series of W-M profiles to explain the periodicity in Fig. 2b. In the figure, the black curve represents the W-M fractal profile with $H = 0.9$, $A = 460$, and random seed (the random seed is a computer terminology, which has the same meaning here. As the initial condition for generating random numbers, random seed dominates the random sequences. Taking ϕ_n in Eq. (7) as an example, $\{\phi_1, \phi_2, \dots, \phi_n\}$ is a random sequence. Once its random seed is determined, the numbers in the sequence are uniquely fixed.) of 11. There are approximately five peaks and five valleys on this rough profile, which means that the profile has approximately five periods. This corresponds to the period in the W-M function. With $N_l = 4$, the period equals $2\pi/(2\pi\gamma^4/L_s) = L_s/\gamma^4 \approx 404.54$. Thus, the wavenumber of the profile is $2048/404.54 \approx 5.06$.

Fig. 3 Comparison of W-M profiles of different Hurst exponents when $N_l = -80$



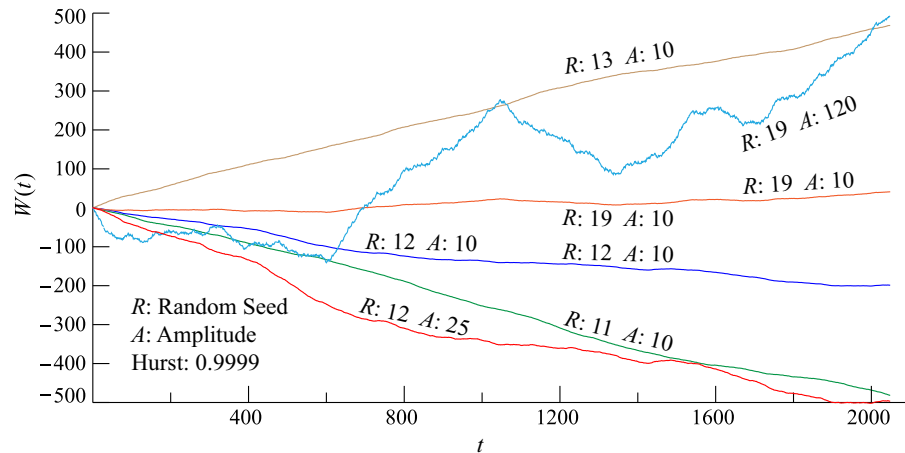
The blue curve in the figure is the cosine curve in the W-M function with both N_l and N_h being 4. The rough profile has a similar trend to that of the blue cosine curve. The five light blue vertical lines separate the profile and the cosine curve into five parts with the same horizontal length.

As in Sects. 2.1 and 2.2, H has controlling effects on the trend between the two steps. Thus, we compared the profile morphology of different Hurst exponents (noted by curves of different colors) in Fig. 2a. Research has found that many natural rock fractures have a small Hurst exponent of approximately 0.8 (Auradou 2009; Odling 1994). In addition, some studies found that the Hurst exponent of natural fractures is less than 0.5 (Babadagli et al 2015; Seybold et al 2020). Thus, in our research, the interval of the Hurst exponent changes from 0.5 to 0.9999. The profiles in the figure have the same A and random seed but different H . In the figure, the smoothest rough profile is represented by the light blue curve ($H = 0.9999$). This profile is a fluctuating rough curve rather than a relatively straight line. However, in terms of fractal theory, when H is close to 1, the fractal object degenerates to a Euclidean object (a straight line). The discrepancy between fractal theory and this phenomenon is caused by the scale of the sampling length and the period scale (Zuo et al 2020). These two scales are both 2048 for the W-M function with $N_l = 0$ and $L_s = 2048$. If the scale of the sampling length approaches or is larger than the period scale, the rough profile exhibits a fluctuating phenomenon with roughness similar to the light blue curve in Fig. 2a or the black profile in (b).

How to resolve this discrepancy becomes crucial to its application in scientific research. From the above paragraph, we know that the discrepancy is caused by the large scale of the sampling length and the small period scale. This problem of the W-M function has also been discussed in Zuo et al (2020), where they indicated that the sampling length plays an important role in affecting the estimation of fractal dimensions. In Fig. 3, the N_l of the profiles was set at -80 to ensure that the period $2\pi / (2\pi\gamma^{-80} / L_s) = L_s / \gamma^{-80} \approx 2.504 \times 10^{17}$ is much larger than 2048. The morphology of profiles with $H = 0.5$ and $H = 0.7$ in the figure is similar to those with corresponding H in Fig. 2a. However, for profiles with $H = 0.9$ and 0.9999 , their fluctuation is smaller than profiles with $N_l = 0$ in Fig. 2a. Obviously, the profile with $H = 0.9999$ is relatively smooth. This comparison indicates that by decreasing the lower limit of the summation, one can obtain a relatively smooth profile with H approximately equal to 1.

To further verify the phenomenon, in Fig. 4, we compare the profiles with $H = 0.9999$ but different random seeds. The A of the profiles is 10, and their morphology with random seeds of 11, 12, 13, and 19 is quite smooth but with different trends: $R = 13$ is positive, while $R = 11$ and $R = 12$ are negative, with the latter having a gentle slope. When $R = 19$, the line is almost around the x -axis. It is known that ϕ_n in Eq. 7 determines the initial phase of cosines and therefore dominates the morphology of rough profiles. The difference in random series is the reason for the different trends of these four profiles. This

Fig. 4 Comparison of W-M profiles with different random seeds when $N_l = -80$



phenomenon can also be explained using Fig. 2b. Since the sampling length is much smaller than the period, the sampling length is only a small part of the whole period. In Fig. 2b, the period is 404.54; here, the sampling length could be a much smaller value, such as 0.1. This short piece may be located at any position in the period. For example, if we set the sampling length as 0.01 on the rough profile in Fig. 2b, the rough profile could be distributed at the peak or valley with a relatively gentle trend, or it may be distributed on mountainsides with a steep slope. This means that when the sampling length is much shorter than the period, the profile shape will be obviously affected by ϕ_n .

In addition to ϕ_n , A becomes another important factor affecting the roughness of W-M fractal profiles. In Fig. 4, two pairs of profiles with different values of A are compared. The A values of the blue curve and the red curve are 10 and 25, respectively. Obviously, the red curve exhibits a steeper trend than the blue curve with $A = 10$. This effect could be better reflected from the comparison between the profile ($R = 19$, $A = 10$) and another profile ($R = 19$, $A = 120$). Their Hurst exponents are all 0.9999, and the profile with $A = 10$ is almost smooth with a small slope around the x -axis; however, the profile with $A = 120$ has an obvious fluctuation and rough features. Compared with the other five curves in Fig. 4, the profile with $A = 120$ is rougher with small spikes.

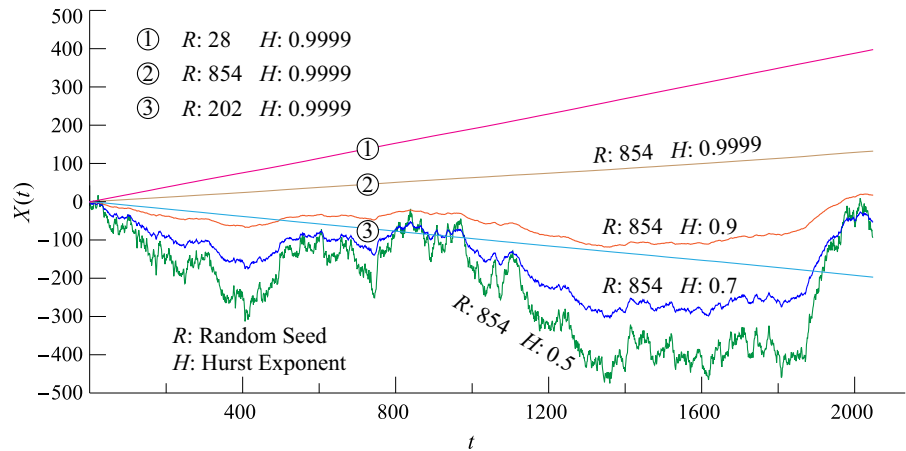
After these comparisons, it is known that the morphology of the W-M rough profiles is controlled by several parameters. Therefore, similar to results noted by other researchers, the W-M function should be

carefully examined before its application. Subsequent comparisons with the FBM profile will be presented. FBM is also a random process; thus, the morphology of profiles varies with the random seed as well. The circled 1, 2, and 3 in Fig. 5 represent FBM graphs with random seeds of 28, 854, and 202, respectively. The Hurst exponent of these three profiles is 0.9999. The difference of random seeds causes different slopes to the profiles. These three approximately straight line profiles are different from those in Figs. 2 and 3. The profiles with $H = 0.9999$ perform like straight lines and are more in line with fractal theory.

In addition to random seeds, profiles of different Hurst exponents are compared in Fig. 5. From top to bottom, the Hurst exponents of the profiles are 0.9999, 0.9, 0.7, and 0.5. These profiles have the same random seed 854, and their roughness increases gradually. When comparing these FBM profiles with the W-M profiles in Fig. 3, one can see that the two kinds of profiles are similar; however, the profiles of these two functions have some differences for a large H .

From all the comparisons above, it is apparent that both FBM and the W-M function are able to construct fractal profiles with randomized characteristics. From the W-M function and FBM construction process, it is identified that there are more controlling parameters in the W-M function, including H , N_l , A , L_s , ϕ_n , and the sampling length. Thus, this function should be carefully checked before its applications. The key point is to ensure a much smaller sampling length than the period of the function. An inappropriate parameter application may cause deviation between

Fig. 5 Comparisons of FBM graphs of different random seeds and different Hurst exponents



the set fractal dimension in the W-M function and the estimated fractal dimension, such as the deviation for profiles with small fractal dimensions in Chen et al (2018). These cases will be discussed in the following analysis.

3.2 Estimation results of the Hurst exponent

To compare the differences between Eqs. (8) and (11), we divided the rough profiles of the W-M function and FBM into multiple segments with the same horizontal scale in each partition. The horizontal scale r_h is set from 2 to 1024 (specifically, 2–51, 54, 55, 57, 58, 60, 62, 64, 66, 68, 71, 73, 76, 79, 82, 85, 89, 93, 97, 102, 108, 114, 120, 128, 136, 146, 157, 171, 186, 205, 227, 256, 292, 341, 409, 512, 682, 1024). Note that these values are selected to ensure that each piece has a similar length. As is known, one profile has a fixed horizontal length; thus, the last piece can only be passively given the remaining length, which may differ from the segment scale. Based on the segmented results, the profile length $L(r_h)$ can therefore be measured. The lengths are listed in Fig. 6, and they increase with the decreasing r_h . From (a) to (d), the segmented rough profiles are FBM with the random seed 202, W-M profiles with $N_l = 4, 0$ and -80 , respectively. The red hexagons, steel blue stars, yellow diamonds, green triangles, dark blue circles, and gray squares in Figs. 6, 7 and 8 represent the length data of profiles with $H = 0.5, 0.6, 0.7, 0.8, 0.9$, and 0.9999 , respectively.

In the figure, it is known that $L(r_h)$ has a power law relationship with r_h , and it decreases heavily with the increase of r_h . In the comparison, (a) and

(d) have similar results and trends. This verified the similarities between FBM and the W-M function (here, we have to note that N_l should be small enough to ensure the scaling rule). The gray squares in both graphs distribute almost horizontally in the bottom, which indicates $L(r_h)$ remains almost stable for different r_h when $H = 0.9999$. This is to say the two profiles perform more like straight lines. The trends of the data in (b) are different from those in (a) and (d). For $N_l = 4$, $\ln(L(r_h))$ is larger and experiences a sudden reduction around $\ln(r_h) = 5$. In addition, for $H = 0.9999$, $L(r_h)$ still shows a clear downward trend rather than a horizontal trend. This phenomenon indicates that the profile is a rough curve similar to the black profile in Fig. 2b. Moreover, the slope is -0.1427 , which is much smaller than -5×10^{-6} in (a) and -0.0012 in (d), respectively. That is, the rough profile with $H = 0.9999$ in (b) has obvious fractal characteristics, which should not be the case for $H \approx 1$. The data in (c) have similar trends to those in (a) or (d); however, the trend of $L(r_h)$ is not horizontal for the gray squares.

$\ln(L(r_h))$ and $\ln(r_h)$ in Fig. 6 have a linear relationship, and their slopes should be $H - 1$ if $L(r) \sim cr^{H-1}$ is met. However, the slopes and H do not satisfy the above relationship, especially for $H = 0.6$ to 0.9 . This indicates that the length Hurst exponent of self-affine profiles is different from the set H . As that has already been derived from Eqs. (9) to (12), for self-affine profiles, the relationship between $L(r_h)$ and r_h is not a simple power law relationship but akin to the relationship in Eq. (10). Here, to verify the relationship between $L(r_h)$ and r_h , we compared the corresponding data in Fig. 7. The vertical axis of these graphs

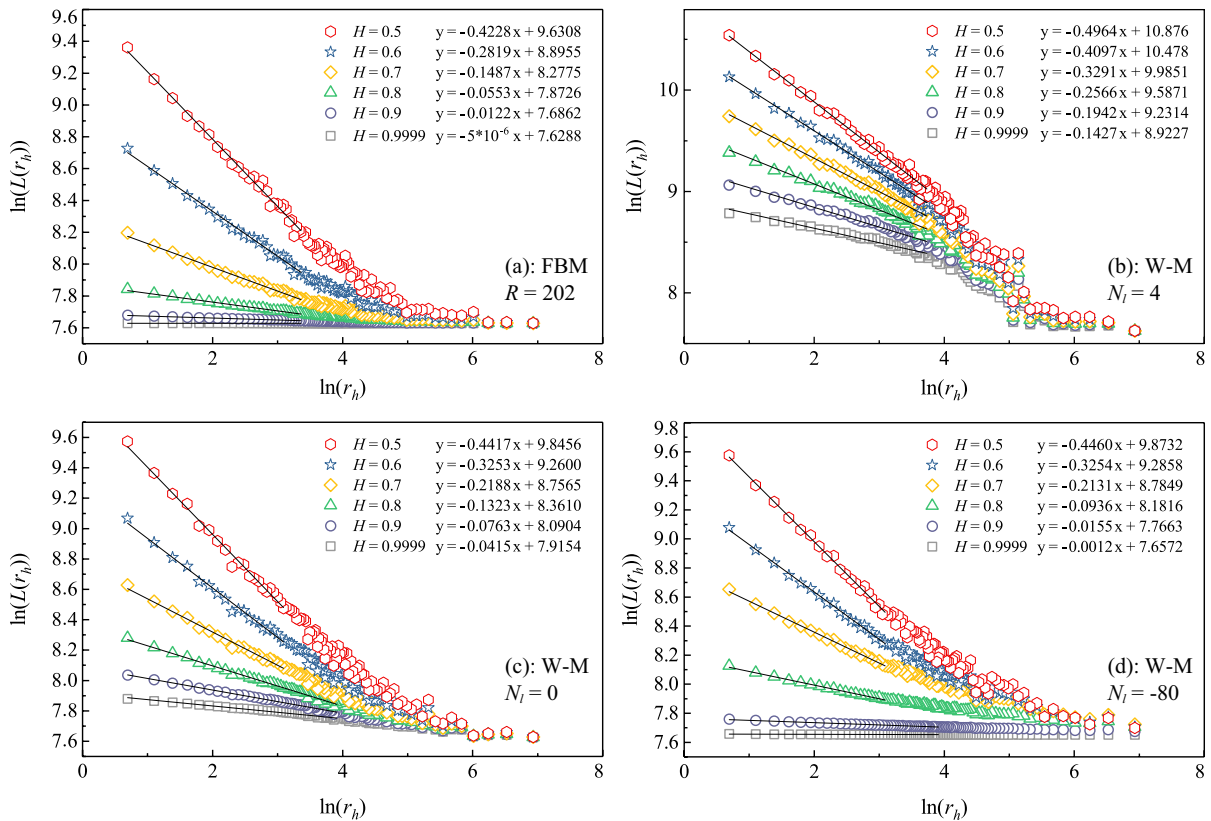


Fig. 6 Power-law relationships between $L(r_h)$ and r_h for FBM and W-M profiles of different H

is $\ln((L(r_h)/\lambda_0)^2 - 1)$. (a) and (d) are similar to the linear relationship from $r_h = 2$ to 1024. For data in (c) with $N_l = 0$, the effective linear interval is smaller than (a) and (d). When $N_l = 4$, the interval decreases, and $\ln((L(r_h)/\lambda_0)^2 - 1)$ experiences a sudden drop at $\ln(r_h) \approx 5.2$. The comparison of these four graphs illustrates that the value of N_l in the W-M function will cause the variation of fractal property in the synthesized profiles.

In Eq. (11), $(L(r_h)/\lambda_0)^2 - 1$ is proportional to r_h^{2H-2} , and therefore, the slopes in Fig. 7 should be equal to $2H - 2$. Combined with the set H , the value of each graph from top to bottom is -1.0 , -0.8 , -0.6 , -0.4 , -0.2 , and -0.0002 . The slopes in (a) and (d) fit these values well. For (b) and (c), the slopes and corresponding $2H - 2$ have a large relative deviation, especially for large H . This further illustrates the impact of N_l on the fractal properties of rough profiles for the W-M function. The above two figures all indicate that the fractal dimension of the W-M function depends not only on the set D in this

function but also on the selection of N_l , N_h , the total length, and the scale interval.

As derived in 2.3, Eq. (11) can be written as the effective vertical length form $v(r_h) = \sigma r_h^H$. This power law relationship is more intuitive and clearer, and, it is convenient for evaluating the H of self-affine profiles. Here, we calculated the effective vertical length using $v(r_h) = \sqrt{l(r_h)^2 - r_h^2}$ and compared the relationship between $\ln(v(r_h))$ and $\ln(r_h)$ in Fig. 8. The random seed of the profiles in (a) is 854.

Different from the trends in the above two figures, $v(r_h)$ in Fig. 8 has an increasing trend with increasing r_h . These linear relationships between $\ln(v(r_h))$ and $\ln(r_h)$ indicate that the power law rule between $v(r_h)$ and r_h . With $v(r_h) = \sigma r_h^H$, it is known that the slope of the linear relationships in the figure should be equal to the set H . The fitted linear interval in (a) and (d) is wide with r_h from 2 to 682. For $N_l = 4$ and $N_l = 0$, the corresponding intervals are much smaller, as can be seen in (b) and (c). In

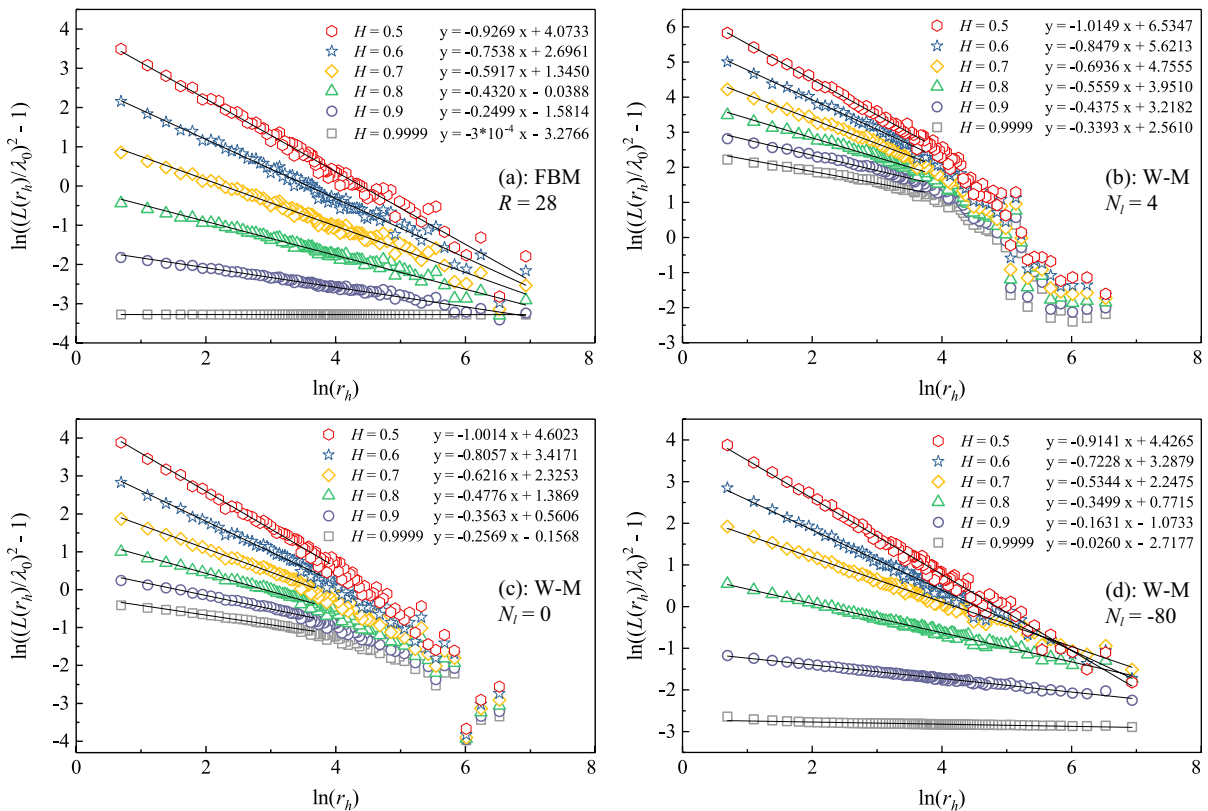


Fig. 7 Power law relationships between $(L(r_h)/\lambda_0)^2 - 1$ and r_h for FBM and W-M profiles of different H

addition, we can see that the slope values in (a) and (d) properly fit the set H . However, the values in (b) and (c) do not match well, especially for large H .

With the data in Figs. 7 and 8, the corresponding Hurst exponents of the FBM and W-M profiles are calculated using Eqs. (11) and (14). Their results are compared in Fig. 9a, where the circles are all distributed near the reference line $y = x$. This result and the derivation in 2.3 indicate Eq. (11) and Eq. (13) have a similar geometric meaning. Note that the length scale relationship is different from Eq. (8). These two models explain the difference between self-affine and self-similarity from the geometric relationship and provide a method for evaluating the H of self-affine profiles.

To verify these two equations and test the fractal properties of the FBM and W-M profiles, we compared the evaluated Hurst exponents and the corresponding set H in Fig. 9b. The calculated Hurst

exponent of FBM profiles with the random seed of 28 is represented by the yellow diamonds, while the green hexagons are the results of W-M profiles with $N_l = -80$, and they all distribute around the line $y = x$. This indicates two points. The first is that the proposed H evaluation method is correct and the evaluated H match the set H well. The other is that the W-M function is able to construct self-affine profiles similar to FBM profiles. However, the results of W-M profiles with $N_l = 4$ and 0 , represented by gray squares and blue stars, are mostly distributed under the line $y = x$, especially for $H \geq 0.7$. In addition, the squares distributed under the stars indicate the evaluated Hurst for W-M profiles of $N_l = 4$ is smaller than that of W-M profiles with $N_l = 0$, and they are both smaller than that of profiles with $N_l = -80$.

The reason for the deviation of H is the inappropriate scale relationship of the W-M function rather than the failure of the Hurst evaluation method. That

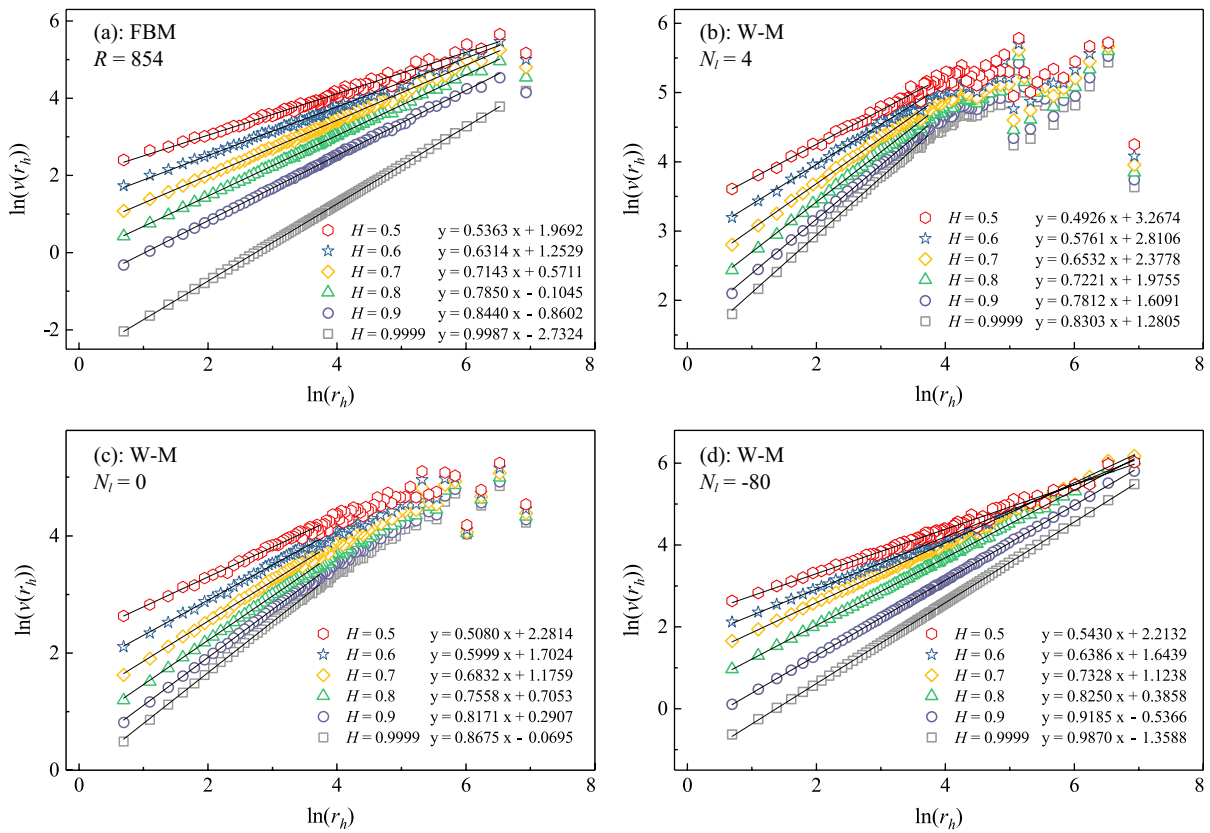


Fig. 8 Power law relationships between $v(r_h)$ and r_h for FBM and W-M profiles of different H

is, the selected N_l in the W-M function is large, which causes the minimum step to be larger. We also plotted the evaluated Hurst exponent of the FBM profiles using Eq. (8) in (b) with the circles that are distributed above $y = x$. This indicates that the evaluated H are larger than the set H and therefore illustrates that the evaluated Hurst exponent using Eq. (8), the traditional length scale relationship, cannot represent the fractal properties of self-affine profiles. Ficker (2017) also pointed out that the fractal dimension of a natural rock joint is unlikely to be as small as that evaluated using the divider method. Equations (11) and (13) provide methods for evaluating the H of self-affine profiles.

4 Conclusions

This research describes the fractal properties of self-affine objects with fractional Brownian motion

and the Weierstrass-Mandelbrot function. The morphology comparison between profiles of FBM and the W-M function verified that the fractal properties of W-M profiles are determined by the controlling parameter (N_l) of low cutoff frequency and the scale length. Only through proper parameters selection can it ensure that the generated profile conforms to the set fractal characteristics. The inappropriate use of parameters is the fundamental cause of deviations in the fractal dimension in some studies. Then, the quantitative fractal model of the self-affine profile length and measurement scale, as well as the fractal relationship between the equivalent vertical height and measurement scale, are derived from the basic geometrical and fractal properties. From the geometric level, it is found that the length $L(r_h)$ of the self-affine profiles at measurement scale r_h satisfies $(L(r_h)/\lambda_0)^2 - 1 = \sigma^2 r_h^{2H-2}$ rather than the simple power law relationship $L(r_h) \sim cr_h^{H-1}$. The

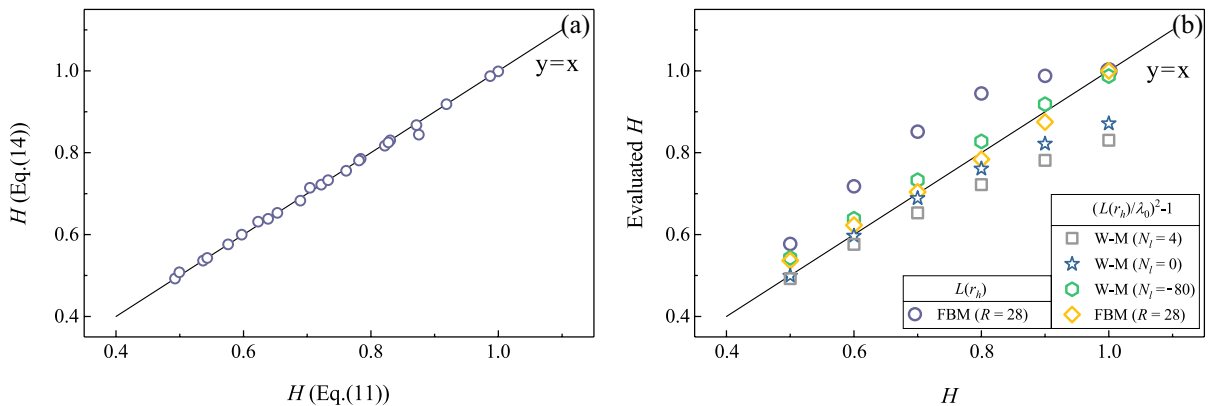


Fig. 9 Verification of the evaluated H . **a** The comparison of Hurst calculated using Eqs. (11) and (14), **b** The Hurst comparison of different rough profiles

complicated relationship between $L(r_h)$ and r_h can be further simplified as a power law relationship between the equivalent vertical height and the measurement scale $v(r_h) = \sigma r_h^H$. All the comparisons show that, compared with the W-M function, FBM has fewer control parameters and therefore is more suitable for the construction of self-affine objects. This paper analyzed the properties of fractal functions (FBM and the W-M function) and their application conditions, which proposes a reference for the correct construction and the H evaluation of the self-affine profiles.

Acknowledgements This work is supported by the Fundamental Research Funds for the Universities of Henan Province (Grant No. NSFRF220427, NSFRF220204), the Doctoral Foundation of Henan Polytechnic University (Grant No. B2021-78), the National Natural Science foundation of China (Grant No. 41972175), the Excellent Youth Foundation of Henan Scientific Committee (Grant No. 232300421025), Natural Science Foundation of Henan Province of China (Grant No. 232300420438), the Program for Innovative Research Team (in Science and Technology) in Universities of Henan Province, China (Grant No. 21IRTSTHN007), the Program for Innovative Research Team (in Science and Technology) of Henan Polytechnic University (Grant No. T2020-4), and the Henan Postdoctoral Foundation.

Declarations

Competing interests The authors have no conflicts of interest to declare that are relevant to the content of this article.

Open Access This article is licensed under a Creative Commons Attribution 4.0 International License, which permits use, sharing, adaptation, distribution and reproduction in any

medium or format, as long as you give appropriate credit to the original author(s) and the source, provide a link to the Creative Commons licence, and indicate if changes were made. The images or other third party material in this article are included in the article's Creative Commons licence, unless indicated otherwise in a credit line to the material. If material is not included in the article's Creative Commons licence and your intended use is not permitted by statutory regulation or exceeds the permitted use, you will need to obtain permission directly from the copyright holder. To view a copy of this licence, visit <http://creativecommons.org/licenses/by/4.0/>.

References

- Auradou H (2009) Influence of wall roughness on the geometrical, mechanical and transport properties of single fractures. *J Phys D Appl Phys* 42(21):214015. <https://doi.org/10.1088/0022-3727/42/21/214015>
- Ausloos M, Berman DH, Victor Berry Michael (1985) A multivariate Weierstrass-Mandelbrot function. *Proceed Royal Soc London A Mathe Phys Sci* 400(1819):331–350. <https://doi.org/10.1098/rspa.1985.0083>
- Babadagli T, Develi K (2003) Fractal characteristics of rocks fractured under tension. *Theoret Appl Fract Mech* 39(1):73–88. [https://doi.org/10.1016/S0167-8442\(02\)00139-8](https://doi.org/10.1016/S0167-8442(02)00139-8)
- Babadagli T, Ren X, Develi K (2015) Effects of fractal surface roughness and lithology on single and multiphase flow in a single fracture: an experimental investigation. *Int J Multiph Flow* 68:40–58. <https://doi.org/10.1016/j.ijmultiphaseflow.2014.10.004>
- Ban L, Du W, Qi C et al (2021) Modified 2D roughness parameters for rock joints at two different scales and their correlation with JRC. *Int J Rock Mech Min Sci* 137(104):549. <https://doi.org/10.1016/j.ijrmm.2020.104549>

- Berry MV, Lewis ZV, Nye JF (1980) On the Weierstrass-Mandelbrot fractal function. *Proceedings of the Royal Society of London A Mathematical and Physical Sciences* 370(1743):459–484. <https://doi.org/10.1098/rspa.1980.0044>
- Brown SR (1987) A note on the description of surface roughness using fractal dimension. *Geophys Res Lett* 14(11):1095–1098. <https://doi.org/10.1029/GL014011p01095>
- Cai J, Lin D, Singh H et al (2018) Shale gas transport model in 3D fractal porous media with variable pore sizes. *Mar Pet Geol* 98:437–447. <https://doi.org/10.1016/j.marpetgeo.2018.08.040>
- Cai Y, Liu D, Pan Z et al (2013) Pore structure and its impact on CH₄ adsorption capacity and flow capability of bituminous and subbituminous coals from Northeast China. *Fuel* 103:258–268. <https://doi.org/10.1016/j.fuel.2012.06.055>
- Chen Z, Liu Y, Zhou P (2018) A comparative study of fractal dimension calculation methods for rough surface profiles. *Chaos, Solitons & Fractals* 112:24–30. <https://doi.org/10.1016/j.chaos.2018.04.027>
- Costa A (2006) Permeability-porosity relationship: A reexamination of the kozeny-carman equation based on a fractal pore-space geometry assumption. *Geophys Res Lett* 33(2):L02318. <https://doi.org/10.1029/2005GL025134>
- Dong J, Ju Y (2020) Quantitative characterization of single-phase flow through rough-walled fractures with variable apertures. *Geomech Geophys Geo-Energy Geo-Resour* 6(3):42. <https://doi.org/10.1007/s40948-020-00166-w>
- Dong J, Ju Y, Gao F et al (2017) Estimation of the fractal dimension of Weierstrass-Mandelbrot function based on cuckoo search methods. *Fractals* 25(06):1750065. <https://doi.org/10.1142/S0218348X17500657>
- Dou Z, Sleep B, Mondal P et al (2018) Temporal mixing behavior of conservative solute transport through 2d self-affine fractures. *Processes* 6(9):158. <https://doi.org/10.3390/pr6090158>
- Dou Z, Zhou Z, Wang J et al (2018) Roughness scale dependence of the relationship between tracer longitudinal dispersion and pecllet number in variable-aperture fractures. *Hydrol Process* 32(10):1461–1475. <https://doi.org/10.1002/hyp.11505>
- Dou Z, Sleep B, Zhan H et al (2019) Multiscale roughness influence on conservative solute transport in self-affine fractures. *Int J Heat Mass Transf* 133:606–618. <https://doi.org/10.1016/j.ijheatmasstransfer.2018.12.141>
- Eliazar II, Shlesinger MF (2013) Fractional motions. *Phys Rep* 527(2):101–129. <https://doi.org/10.1016/j.physrep.2013.01.004>
- Falconer KJ (2014) *Fractal geometry: mathematical foundations and applications*, third, edition. Wiley, Hoboken
- Feranie S, Fauzi U, Bijaksana S (2011) 3d fractal dimension and flow properties in the pore structure of geological rocks. *Fractals* 19(03):291–297. <https://doi.org/10.1142/S0218348X1100535X>
- Ficker T (2017) Fractal properties of joint roughness coefficients. *Int J Rock Mech Min Sci* 94:27–31. <https://doi.org/10.1016/j.ijrmm.2017.02.014>
- Ganti S, Bhushan B (1995) Generalized fractal analysis and its applications to engineering surfaces. *Wear* 180(1):17–34. [https://doi.org/10.1016/0043-1648\(94\)06545-4](https://doi.org/10.1016/0043-1648(94)06545-4)
- Gao M, Xie J, Guo J et al (2021) Fractal evolution and connectivity characteristics of mining-induced crack networks in coal masses at different depths. *Geomech Geophys Geo-Energy Geo-Resour* 7(1):9. <https://doi.org/10.1007/s40948-020-00207-4>
- Jin Y, Dong JB, Zhang XY et al (2017) Scale and size effects on fluid flow through self-affine rough fractures. *Int J Heat Mass Transf* 105:443–451. <https://doi.org/10.1016/j.ijheatmasstransfer.2016.10.010>
- Jin Y, Wu Y, Li H et al (2017) Definition of fractal topography to essential understanding of scale-invariance. *Sci Rep* 7(46):672. <https://doi.org/10.1038/srep46672>
- Jin Y, Liu X, Song H et al (2019) General fractal topography: an open mathematical framework to characterize and model mono-scale-invariances. *Nonlinear Dyn* 96(4):2413–2436. <https://doi.org/10.1007/s11071-019-04931-9>
- Jin Y, Wang C, Liu S et al (2020) Systematic definition of complexity assembly in fractal porous media. *Fractals* 28(5):2050079. <https://doi.org/10.1142/S0218348X20500796>
- Ju Y, Dong J, Gao F et al (2019) Evaluation of water permeability of rough fractures based on a self-affine fractal model and optimized segmentation algorithm. *Adv Water Resour* 129:99–111. <https://doi.org/10.1016/j.advwatres.2019.05.007>
- Karle NN, Kolwankar KM (2015) Characterization of the irregularity of a terrain using fractal dimension of lakes' boundaries. *Fractals* 23(02):1550002. <https://doi.org/10.1142/S0218348X15500024>
- Li J, Du Q, Sun C (2009) An improved box-counting method for image fractal dimension estimation. *Pattern Recogn* 42(11):2460–2469. <https://doi.org/10.1016/j.patcog.2009.03.001>
- Liu P, Ju Y, Feng Z et al (2021) Characterization of hydraulic crack initiation of coal seams under the coupling effects of geostress difference and complexity of pre-existing natural fractures. *Geomech Geophys Geo-Energy Geo-Resour* 7(4):91. <https://doi.org/10.1007/s40948-021-00288-9>
- Liu Y, Wang Y, Chen X et al (2017) Two-stage method for fractal dimension calculation of the mechanical equipment rough surface profile based on fractal theory. *Chaos Solitons Fractals* 104:495–502. <https://doi.org/10.1016/j.chaos.2017.09.012>
- Magdziarz M, Weron A, Burnecki K et al (2009) Fractional Brownian Motion versus the continuous-time random walk: a simple test for subdiffusive dynamics. *Phys Rev Lett* 103(18):180602. <https://doi.org/10.1103/PhysRevLett.103.180602>
- Mandelbrot B (1967) How long is the coast of Britain? Statistical self-similarity and fractional dimension. *Science* 156(3775):636–638. <https://doi.org/10.1126/science.156.3775.636>
- Mandelbrot BB (1977) *Fractals: Form, Chance, and Dimension*. Freeman, San Francisco
- Mandelbrot BB, Van Ness JW (1968) Fractional Brownian motions, fractional noises and applications. *SIAM Rev* 10(4):422–437. <https://doi.org/10.1137/1010093>
- Odling NE (1994) Natural fracture profiles, fractal dimension and joint roughness coefficients. *Rock Mech Rock Eng* 27(3):135–153. <https://doi.org/10.1007/BF01020307>

- Pinnington RJ (2012) A particle-envelope surface model for road- tyre interaction. *Int J Solids Struct* 49(3–4):546–555. <https://doi.org/10.1016/j.ijsolstr.2011.10.022>
- Seybold HJ, Carmona HA, Filho FAL et al (2020) Flow through three-dimensional self-affine fractures. *Phys Rev Fluids* 5(10):104101. <https://doi.org/10.1103/PhysRevFluids.5.104101>
- Sugihara G, Grenfell B, May RM (1990) Distinguishing error from chaos in ecological time-series. *Philos Trans R Soc Lond B Biol Sci* 330(1257):235–251. <https://doi.org/10.1098/rstb.1990.0195>
- Ünlüsoy D, Süzen ML (2020) A new method for automated estimation of joint roughness coefficient for 2D surface profiles using power spectral density. *Int J Rock Mech Min Sci* 125(104):156. <https://doi.org/10.1016/j.ijrmms.2019.104156>
- Wiener N (1923) Differential-Space. *J Math Phys* 2(1–4):131–174. <https://doi.org/10.1002/sapm192321131>
- Wong Pz (1987) Fractal surfaces in porous media. In: *AIP Conference Proceedings*, vol 154. AIP, pp 304–317. <https://doi.org/10.1063/1.36383>
- Wu JJ (2000) Characterization of fractal surfaces. *Wear* 239(1):36–47. [https://doi.org/10.1016/S0043-1648\(99\)00362-2](https://doi.org/10.1016/S0043-1648(99)00362-2)
- Wu JJ (2002) Analyses and simulation of anisotropic fractal surfaces. *Chaos, Solitons Fractals* 13(9):1791–1806. [https://doi.org/10.1016/S0960-0779\(01\)00192-8](https://doi.org/10.1016/S0960-0779(01)00192-8)
- Xia Y, Cai J, Wei W et al (2018) A new method for calculating fractal dimensions of porous media based on pore size distribution. *Fractals* 26(01):1850006. <https://doi.org/10.1142/S0218348X18500068>
- Xu P (2015) A discussion on fractal models for transport physics of porous media. *Fractals* 23(03):1530001. <https://doi.org/10.1142/S0218348X15300019>
- Xu P, Li C, Qiu S et al (2016) A fractal network model for fractured porous media. *Fractals* 24(02):1650018. <https://doi.org/10.1142/S0218348X16500183>
- Yan W, Komvopoulos K (1998) Contact analysis of elastic-plastic fractal surfaces. *J Appl Phys* 84(7):3617–3624. <https://doi.org/10.1063/1.368536>
- Yang B, Xue L, Duan Y et al (2021) Correlation study between fracability and brittleness of shale-gas reservoir. *Geomech Geophys Geo-Energy Geo-Resour* 7(2):31. <https://doi.org/10.1007/s40948-021-00231-y>
- Yin X, Komvopoulos K (2010) An adhesive wear model of fractal surfaces in normal contact. *Int J Solids Struct* 47(7):912–921. <https://doi.org/10.1016/j.ijsolstr.2009.12.003>
- Yu B (2006) Fractal dimensions for multiphase fractal media. *Fractals* 14(02):111–118. <https://doi.org/10.1142/S0218348X06003155>
- Yu B, Li J (2001) Some fractal characters of porous media. *Fractals* 09(03):365–372. <https://doi.org/10.1142/S0218348X01000804>
- Zhang D, Gao H, Dong Q et al (2021) Numerical study of forward and reverse flow characteristics of rough-walled tree-like fracture networks. *Geomech Geophys Geo-Energy Geo-Resour* 7(3):63. <https://doi.org/10.1007/s40948-021-00260-7>
- Zhang Q, Luo S, Ma H et al (2019) Simulation on the water flow affected by the shape and density of roughness elements in a single rough fracture. *J Hydrol* 573:456–468. <https://doi.org/10.1016/j.jhydrol.2019.03.069>
- Zhang Q, Luo S, Ma H et al (2020) Experimental study on quantifying the surface form of artificial tension fractures in granite samples. *J Hydrol* 584(124):680. <https://doi.org/10.1016/j.jhydrol.2020.124680>
- Zhao L, Zhang S, Huang D et al (2018) Quantitative characterization of joint roughness based on semivariogram parameters. *Int J Rock Mech Min Sci* 109:1–8. <https://doi.org/10.1016/j.ijrmms.2018.06.008>
- Zhao M, Jin Y, Liu X et al (2020) Characterizing the complexity assembly of pore structure in a coal matrix: Principle, Methodology, and modeling application. *J Geophys Res Solid Earth*. <https://doi.org/10.1029/2020JB020110>
- Zhao Y, Zhang C, Wang Y et al (2021) Shear-related roughness classification and strength model of natural rock joint based on fuzzy comprehensive evaluation. *Int J Rock Mech Min Sci* 137(104):550. <https://doi.org/10.1016/j.ijrmms.2020.104550>
- Zheng J, Jin Y, Liu X et al (2020) Validity of triple-effect model for fluid flow in mismatched, self-affine fractures. *Adv Water Resour* 140(103):585. <https://doi.org/10.1016/j.advwatres.2020.103585>
- Zhou Y, Li Y, Zhu H et al (2015) The three-point sinuosity method for calculating the fractal dimension of machined surface profile. *Fractals* 23(02):1550016. <https://doi.org/10.1142/S0218348X15500164>
- Zimmerman RW, Kumar S, Bodvarsson GS (1991) Lubrication theory analysis of the permeability of rough-walled fractures. *Int J Rock Mech Mining Sci Geomech Abstracts* 28(4):325–331. [https://doi.org/10.1016/0148-9062\(91\)90597-F](https://doi.org/10.1016/0148-9062(91)90597-F)
- Zuo X, Zhu H, Zhou Y et al (2015) A new method for calculating the fractal dimension of surface topography. *Fractals* 23(03):1550022. <https://doi.org/10.1142/S0218348X1550022X>
- Zuo X, Tang X, Zhou Y (2020) Influence of sampling length on estimated fractal dimension of surface profile. *Chaos Solitons Fractals* 135(109):755. <https://doi.org/10.1016/j.chaos.2020.109755>